
How does longer temporal context enhance multimodal narrative video processing in the brain?

Prachi Jindal^{1,*}, Anant Khandelwal^{2,*}, Manish Gupta³,

Bapi S. Raju⁴, Subba Reddy Oota⁵, Tanmoy Chakraborty¹

¹IIT Delhi, India, ²Microsoft Research, Bangalore, India, ³Microsoft, India

⁴IIT-Hyderabad, India, ⁵Technische Universität Berlin, Germany

prachi.jindal19561@gmail.com, {anantk, gmanish}@microsoft.com

raju.bapi@iitd.ac.in, subba.reddy.ota@tu-berlin.de, tanchak@iitd.ac.in

Abstract

Understanding how humans and artificial intelligence systems process complex narrative videos is a fundamental challenge at the intersection of neuroscience and machine learning. This study investigates how the temporal context length of video clips (3–12 s clips) and the narrative-task prompting shape brain-model alignment during naturalistic movie watching. Using fMRI recordings from participants viewing full-length movies, we examine how brain regions sensitive to narrative context dynamically represent information over varying timescales and how these neural patterns align with model-derived features. We find that increasing clip duration substantially improves brain alignment for multimodal large language models (MLLMs), whereas unimodal video models show little to no gain. Further, shorter temporal windows align with perceptual and early language regions, while longer windows preferentially align higher-order integrative regions, mirrored by a layer-to-cortex hierarchy in MLLMs. Finally, narrative-task prompts (multi-scene summary, narrative summary, character motivation, and event boundary detection) elicit task-specific, region-dependent brain alignment patterns and context-dependent shifts in clip-level tuning in higher-order regions. Together, our results position long-form narrative movies as a principled testbed for probing biologically relevant temporal integration and interpretable representations in long-context MLLMs.

1 Introduction

The alignment between internal representations of Transformer-based models and cortical activation patterns elicited by naturalistic stimuli has emerged as a key focus in the study of brain-model correspondence (Toneva & Wehbe, 2019; Schrimpf et al., 2021; Caucheteux & King, 2022; Oota et al., 2025a; Goldstein et al., 2025). In particular, prior work has demonstrated that contextual representations extracted from such Transformer models outperform static word embeddings, offering improved brain alignment and capturing temporal dynamics across model depth in both text (Toneva & Wehbe, 2019) and speech (Vaidya et al., 2022; Oota et al., 2024). More recently, multimodal Transformer models have been shown to achieve a higher degree of brain predictivity across various stimulus modalities (Nakagi et al., 2024; Subramaniam et al., 2024; Dong & Toneva, 2023a; Oota et al., 2025d; Sartzetaki et al., 2025). However, the role of longer temporal context in brain alignment for naturalistic multimodal stimuli remains underexplored. Therefore, extending these insights to naturalistic narrative movies is important because comprehension depends on integrating information over longer timescales.

*Equal contribution

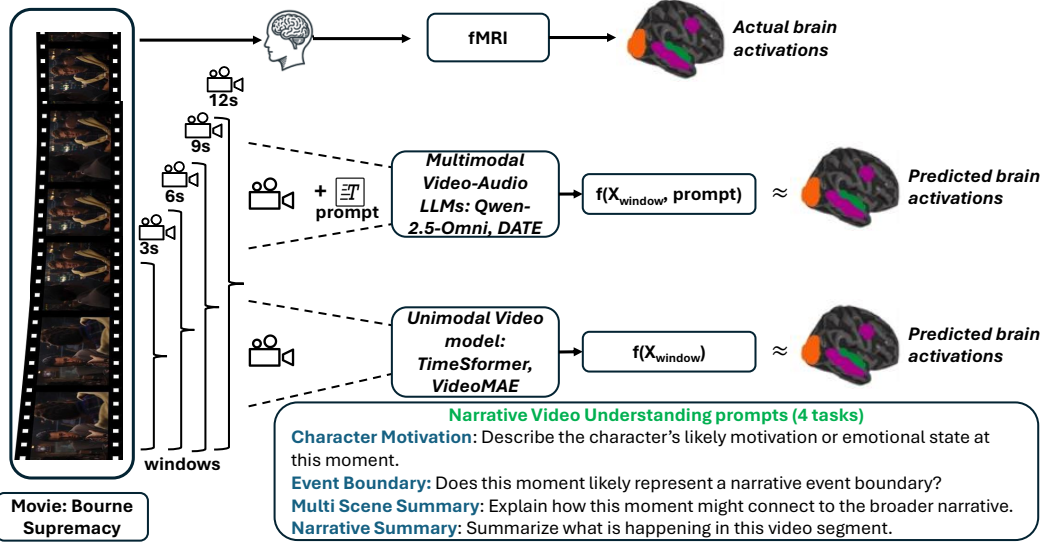


Figure 1: Leveraging temporal video context of different durations (X_{windows}) with unimodal and multimodal models for brain encoding with a diverse set of instructions (prompts). We experiment with 4 narrative video understanding tasks: character motivation, event boundary detection, multi-scene summarization, narrative summarization.

Understanding how narrative videos are processed by both AI models and the human brain is an important open problem in cognitive neuroscience and AI. Humans seamlessly integrate visual scenes and the context of the story over time, drawing on sight and sound to comprehend movies. For current AI models, this remains challenging: earlier video Transformer models often processed videos as frame sequences with limited context windows. Processing long sequences of frames are computationally expensive and can exceed memory constraints, hence earlier models often resort to subsampling frames or truncating context. Consequently, previous *multimodal* brain-encoding studies have typically relied on short clips (e.g., 1.49 s), thereby neglecting extended temporal context (Subramaniam et al., 2024; Dong & Toneva, 2023a; Oota et al., 2025d; Sartzetaki et al., 2025).

Narrative comprehension is a complex cognitive process that involves the integration of visual, auditory, and contextual information over time. In the human brain, this process recruits a hierarchy of cortical regions that operate on multiple temporal scales, from sensory processing of moment-to-moment events to the integration of extended narrative context across scenes and subplots (Lerner et al., 2011; Simony et al., 2016). fMRI studies using continuous movie stimuli have shown that higher-order brain areas, including regions within the default mode network, are especially sensitive to longer narrative contexts, often requiring tens of seconds of uninterrupted input to represent story-level meaning Baldassano et al. (2018); Khosla et al. (2021). This motivates evaluating brain alignment of video–audio models on naturalistic movies while systematically increasing the temporal context window.

Using brain recordings of participants watching several popular movies with audio (Boyle et al., 2020), we investigate the brain alignment of two pretrained video-audio MLLMs. Specifically, as shown in Fig. 1, we evaluate Qwen-2.5-Omni (Xu et al., 2025) and DATE (Yuan et al., 2025), which are end-to-end multimodal models that jointly process video and audio in an interleaved way, rather than treating them separately. We also experiment with two unimodal video models (TimeSFormer (Bertasius et al., 2021) and VideoMAE (Tong et al., 2022)). We evaluate four narrative video understanding tasks and vary the temporal context using clip duration (3s, 6s, 9s, and 12s) and estimate brain alignment across tasks and temporal context. Overall, this study addresses the following research questions:

RQ1 How does increasing the temporal context-length (3–12 s clip duration) affect the brain predictivity of video-audio MLLM and unimodal video model representations during naturalistic movie watching?

- RQ2 Which brain regions show the largest gains (or shifts in optimal window length) in brain predictivity as the temporal context increases, and how are these effects related to the layer-wise representations of video–audio MLLMs?
- RQ3 Which narrative-task instructions (character motivation, event boundary detection, multi-scene summary, and narrative summary) exhibit the highest brain-alignment of MLLM representations during naturalistic movie watching, and do these task-specific representations dissociate into distinct ROI-specific patterns?
- RQ4 Which video clips are most predictive of voxel responses across temporal context lengths and narrative tasks, and how do these patterns vary across ROIs?

Our analysis of longer temporal context and narrative-task prompting in video-audio MLLMs yields several key conclusions corresponding to the RQs:

- A1 Increasing temporal context (clip duration from 3 s to 12 s) systematically improves brain predictivity for video-audio MLLMs, while unimodal video models show little to no improvement with longer context windows.
- A2 We find an ROI-specific (region of interest) temporal gradient: longer temporal windows align best with higher-order semantic regions (e.g., posterior cingulate cortex (PCC)), whereas shorter-to-intermediate windows (3–6 s) are optimal for perceptual and early language regions (e.g., posterior temporal lobe (PTL)), mirroring a layer-wise hierarchy in MLLMs.
- A3 Probing MLLMs with narrative task instructions reveals that (*Narrative Summary* and *Multi-scene Summary*) explain a larger portion of voxels in higher-order language ROIs, while *Character Motivation* preferentially aligns with more localized temporal language regions; suggesting that task instructions can be used as functional probes of brain-aligned representations.
- A4 Interpretation of video clips that most strongly drive voxel responses show that the maximally activating clips are largely the same across temporal windows in visual ROIs, but change with temporal context in higher-order language ROIs.

Overall, these results demonstrate that temporal context and narrative-task prompting act as complementary probes for long-form narrative video understanding in the brain, and for interpreting long-context representations in video-audio MLLMs. We present one of the first systematic evaluations of extended temporal context and narrative-task prompting in video–audio MLLMs, showing that context- and task-dependent representations are associated with distinct patterns of brain alignment across cortical regions and model layers. The code is part of supplementary material.

2 Related Work

Contextual Representations and Brain Alignment. Our work is most closely related to studies by Jain & Huth (2018); Toneva & Wehbe (2019); Aw & Toneva (2023); Vaidya et al. (2022); Oota et al. (2024), who investigate how high-level contextual representations from modern language models map onto human brain activity, and examine how contextual dynamics affect brain–model alignment in language-related ROIs. Jain & Huth (2018); Toneva & Wehbe (2019); Aw & Toneva (2023) focus on text-based language models with context lengths ranging from 1 to 500 words, whereas Vaidya et al. (2022); Oota et al. (2024) study speech-based models with context windows ranging from 1.49 to 64 seconds. Beyond text and speech, a growing body of work models brain responses during naturalistic movie viewing using representations from unimodal and multimodal models, and more recently from MLLMs, providing strong baselines for video-to-brain encoding (Dong & Toneva, 2023a,b; Oota et al., 2025b,d). Motivated by these studies, we extend this line of work to naturalistic videos by testing how long-range visual context shapes brain–model alignment, comparing unimodal video encoders and MLLMs.

Multimodal Brain Encoding. Our work also relates to a growing literature on aligning AI model representations with human brain activity under naturalistic stimuli. Several studies have used unimodal video models and multimodal models (e.g., video+audio) to predict movie-evoked brain activity with strong predictive performance (Dong & Toneva, 2023a,b; Oota et al., 2025d). We summarize representative evaluation settings, particularly stimulus modality and temporal window length in Table 1. However, much of this prior multimodal work relies on short clips or limited temporal windows, which can underrepresent the role of extended temporal context in naturalistic

Table 1: Overview of multimodal model evaluation settings in brain encoding studies.

Study	Model Type	Stimulus Modality	Brain Data	Dataset	Video Len
Popham et al. (2021)	Vision-Only CNNs vs. Vision-Language	Unimodal (Silent Videos)	fMRI	Gallant lab short video clips	2s
Tang et al. (2024)	Non-instruction-tuned multimodal model (BridgeTower)	Unimodal (Silent Videos), Unimodal (listening stories)	fMRI	Gallant lab short video clips	2s
Subramanian et al. (2024)	Non-instruction-tuned multimodal models (SLIP, CLIP, SimCLR, BLIP, BEiT)	Image frame-text pairs (Movies)	SEEG	AMMT	4s
Lahmer et al. (2024)	Resnet50 with Temporal Shift Module	Video clips	fMRI	BOLD Moments	3s
Dong & Toneva (2023a)	Non-instruction-tuned multimodal models (MER, LOT Reserve)	Multimodal (Movies: Videos with audio)	fMRI	Neuromod Friends dataset	35s
Oota et al. (2025d)	Non-instruction-tuned multimodal models (TVLT and ImageBind)	Multimodal (Movies: Videos with audio)	fMRI	Neuromod Movie10	1.49s
Sartetaki et al. (2025)	Object and Action recognition models	Image frames to CNNs, Video clips to video models	fMRI	BOLD Moments	3s
Oota et al. (2025c)	Instruction-tuned video and audio MLLMs	Multimodal (Movies: Videos with audio)	fMRI	Neuromod Movie10	1.49s
Ours	Unimodal Video models and Video-based MLLMs	Multimodal (Movies: Videos with audio)	fMRI	Neuromod Movie10	3s - 12s

video understanding. Complementary to these efforts, our work builds on and extends this line of work by proposing an architecture-agnostic evaluation protocol to characterize context- and instruction-dependent representational changes across varying time windows and tasks, and relate these changes to brain alignment.

3 Dataset Curation and Tasks

3.1 Brain imaging dataset

We experiment with Movie10 (Boyle et al., 2020), a multimodal naturalistic fMRI dataset, obtained from the Courtois NeuroMod databank. This dataset was collected while four human subjects (s1, s2, s3, s5; data for s4 and s6 is not public) passively watched four different movies: *The Bourne supremacy*, *The wolf of wall street*, *Hidden figures* and *Life*. Among these, *Hidden figures* and *Life* are repeated twice, with the repeats used for testing and the remaining movies for training. In this work, we use *Life* movies for testing where we average the two repetitions to reduce noise in brain data. The dataset includes 11,017 TRs (Repetition Time) for training and 2013 TRs for testing. We build encoding models where the train and test sets are totally disjoint. The fMRI data is collected every 1.49 seconds (= 1 TR). More details about dataset and preprocessing are in Appendix A.

The dataset is already preprocessed and projected onto the surface space (“fsaverage6”). We use the multimodal parcellation of the human cerebral cortex based on the Glasser Atlas (which consists of 180 regions of interest in each hemisphere) to report the ROI analysis for the brain maps (Glasser et al., 2016). We select our language ROIs based on the Fedorenko lab’s language parcels (Milton et al., 2021; Desai et al., 2023). We show the flatmap with labeled ROIs in Appendix Fig. 8 and list the detailed sub-ROIs of these ROIs in Appendix A.

Estimating cross-subject prediction accuracy. To account for intrinsic noise in biological measurements, we adapt the method of Schrimpf et al. (2021); Oota et al. (2024) to estimate the cross-subject prediction accuracy for a model’s performance for the Movie10 fMRI dataset. Each subject $s \in (s1, s2, s3, s5)$ is chosen as the prediction target and the other three are used to predict this target. Note that the estimated cross-subject prediction accuracy is based on the assumption of a perfect model, which might differ from real-world scenarios, yet offers valuable insights into model’s performance. We present the cross-subject prediction accuracy across voxels for the Movie10 fMRI dataset for each of the four participants in Appendix B.

3.2 Motivation for Narrative Tasks

We focus on four core narrative tasks (Character Motivation, Event Boundary Detection, Multi-Scene Summary, and Narrative Summary; see the task instructions in Table 2) because together they capture the complementary and irreducible components of narrative understanding. This choice rests on three mild assumptions. First, narrative comprehension can be decomposed into local semantics, agent-centric inference, temporal segmentation, and cross-scene integration Bruner (1991); Abbott (2008). Second, a task-conditioned multimodal model is capable of recovering each component Zellers et al. (2021); Gupta et al. (2022). Third, the outputs of these tasks can be linearly, or through a low-dimensional nonlinear readout, composed into downstream predictions Schwartz et al. (2022).

Empirical evidence further supports that neuroimaging studies demonstrate that different cortical regions align with these narrative components, and that combining task outputs improves voxel-level

Table 2: Instructions for multimodal narrative understanding tasks.

Task	Description
Character Motivation	Based on this given video segment, describe the character’s likely motivation or emotional state at this moment. Justify your answer using visual or contextual cues.
Event Boundary Detection	You are shown a video segment from a larger movie. Based only on this segment, does this moment likely represent a narrative event boundary, such as a scene change?
Multi Scene Summary	You are shown a video segment from a larger movie. Based only on this clip, explain how this moment might connect to the broader narrative.
Narrative Summary	Summarize what is happening in this video segment. Clearly describe the observed events, characters, and any inferences about the context.

prediction of brain activity during story comprehension Huth et al. (2016); Honey et al. (2012); Wehbe et al. (2014). We provide detailed description about each narrative task in Appendix C.

4 Methodology

4.1 Multimodal Large Language Models (MLLMs)

Since humans are capable of simultaneously perceiving the visual and auditory information while watching movies, to investigate long narrative video understanding, we use two pretrained video+text MLLMs, each containing 36 layers: (i) Qwen-2.5-Omni model (Xu et al., 2025), an end-to-end multimodal model that processes video and audio together in an interleaved way, rather than treating them separately, and (ii) DATE (Dynamic Absolute Time Enhancement) model (Yuan et al., 2025) built on Qwen-2.5-VL model, a plug-and-play framework to improve the capabilities of MLLMs in understanding long videos, particularly for tasks that require precise temporal reasoning and event localization. When prompted with narrative task instructions, these models produce task-specific multimodal representations that we use for brain encoding.

Extraction of Temporal Context from Long Videos. To extract narrative task representations from a MLLM, we use a sliding-window procedure to define temporally coherent segments. We extract consecutive windows of length W seconds with a stride of 1.49 s, resulting in overlapping temporal segments. Each window was treated as a contiguous video snippet and paired with a narrative task instruction before being passed to the MLLMs. From every segment, the processor uniformly sampled number of frames (16 frames per window), together with synchronized audio to capture richer temporal dynamics. The model produced hidden state representations across all Transformer layers during token generation; these were averaged across tokens at each layer to yield a compact embedding per layer for each sliding window with respect to task instruction. For the two MLLMs, we use the pretrained Transformer model weights for extracting representations.

4.2 Unimodal Video Baselines

We also compare with two unimodal video models, VideoMAE (Tong et al., 2022) and TimeSFormer (Bertasius et al., 2021) each with 12 layers. For each video clip, we extract layer-wise hidden state representations using the same sliding-window approach as for MLLMs, but without any task prompts (video-only input). We average these hidden states to obtain a single embedding per layer for each sliding window, and use these embeddings for brain encoding.

5 Experiments

5.1 Experimental Setup

Encoding model. We train bootstrap ridge regression based voxel-wise encoding models (Deniz et al., 2019) to predict the fMRI brain activity associated with the stimulus representations obtained from the 4 narrative task-specific instructions for both multimodal LLMs. We employ z-score thresholding separately for both input stimulus representations and brain recordings for training and test datasets. This helps identify and remove extreme outliers that could disproportionately affect the Pearson Correlation results. For each subject, we account for the delay in the hemodynamic response by modeling the hemodynamic response function using a finite response filter (FIR) per voxel with 5 temporal delays (TR) corresponding to ~ 7.5 seconds (Huth et al., 2022). Formally, at each time step

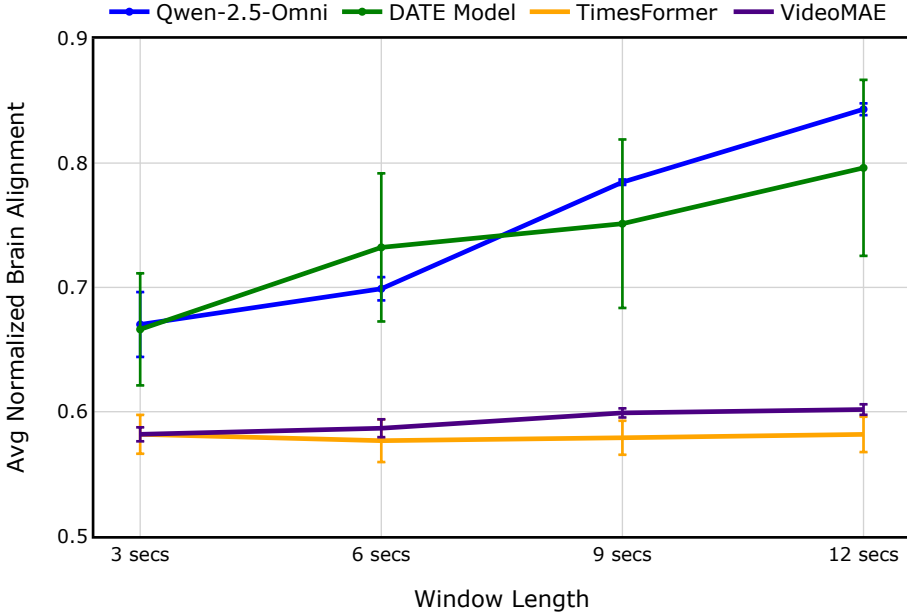


Figure 2: Average normalized brain alignment as a function of temporal window length (3 to 12s) for MLLMs, and unimodal video baselines. MLLMs show increasing alignment with longer windows, while unimodal video models remain approximately constant. Error bars denote variability across subjects (mean \pm standard error of the mean).

t , we encode the stimuli as $X_t \in \mathbb{R}^D$ and voxels from the brain region $Y_t \in \mathbb{R}^V$, where D denotes the dimension of the concatenation of 5 delayed TRs and V denotes the number of voxels.

Train-test setup. We build encoding models where the train and test sets are totally disjoint and the model cannot use any clock relationships from the training data during inference. To be completely clear: independent encoding models are trained for each subject using data concatenated from two movies (11017 TRs). The test set consisted only of data from the “*Life*” movie (2028 TRs). Thus, there is no possibility of any information leakage during inference on the test set. Hyper-parameter settings are in Appendix D.

Evaluation metrics. We evaluate our models using Pearson Correlation (PC), which is a standard metric to evaluate brain alignment (Jain & Huth, 2018; Schrimpf et al., 2021; Goldstein et al., 2022). Let TR be the number of time repetitions in the test set. Let $Y = \{Y_i\}_{i=1}^{TR}$ and $\hat{Y} = \{\hat{Y}_i\}_{i=1}^{TR}$ denote the actual and predicted value vectors for a single voxel, respectively. Thus, Y and $\hat{Y} \in \mathbb{R}^{TR}$. We use PC to compute the correlation function, $corr(Y, \hat{Y})$. The final measure of a model’s performance is obtained by calculating Pearson’s correlation between the model’s predictions and neural recordings. To quantify the model predictions, the resulting model prediction correlations are divided by the estimated cross-subject prediction accuracy; and averaged across voxels, regions, and participants, resulting in a standardized measure of performance referred to as normalized brain alignment. To calculate *normalized alignment*, we select voxels with cross-subject prediction accuracy ≥ 0.05 .

5.2 Experimental Evaluation

[A1]: Longer temporal context improves brain predictivity for MLLMs but not for unimodal models.

Avg normalized brain alignment vs. temporal context length. First, we quantify brain predictivity on the Movie10 dataset across the temporal context using representations extracted from video-audio MLLMs and unimodal video baselines (TimeSFormer and VideoMAE), as shown in Fig. 2. For each model, we report the average normalized brain alignment across subjects at the best performing layer (layer 36 for MLLMs and layer 12 for unimodal baselines).

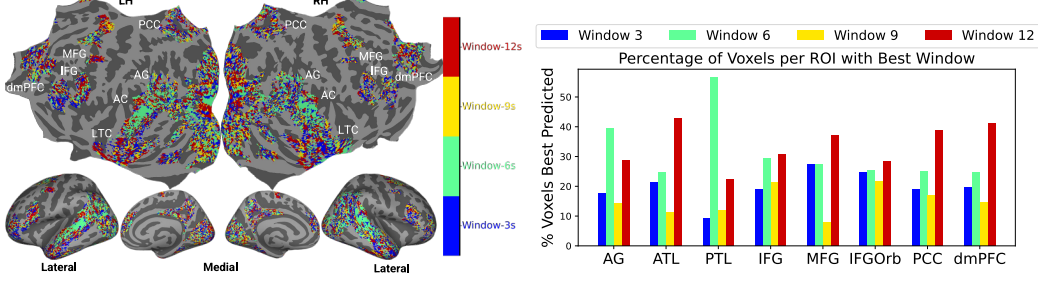


Figure 3: Each voxel is color-coded with the video duration (window length) that led to the highest normalized brain alignment with the Qwen-2.5-Omni model. The color bar highlights color codes for each window length. (Left) The voxels are projected onto the flattened cortical surface of the ‘fsaverage’ subject. (Right): Percentage of best predicted voxels whose brain encoding performance is higher corresponding to each window length within language-selective regions, and visual regions. Results for DATE are in Appendix E.

From Fig. 2, we make the following observations: (i) As context increases from 3 s to 12 s, both Qwen-2.5-Omni ($\sim 26\%$ relative gain; $0.67 \rightarrow 0.84$) and DATE ($\sim 19\%$ relative gain; $0.67 \rightarrow 0.80$) exhibit a consistent increase in brain alignment, whereas unimodal video baselines show little to no change across window lengths ($0.58 \rightarrow 0.60$). Paired two-sided t -tests across subjects ($df = 3$) further show that Qwen-2.5-Omni significantly outperforms the unimodal video baselines at longer contexts (6s: $p = 0.005$; 9s: $p = 8.5 \times 10^{-4}$; 12s: $p = 0.0012$), while the difference at 3s is not significant ($p = 0.107$); DATE shows the same pattern. In contrast, Qwen-2.5-Omni and DATE do not differ significantly at any window length (all $p \geq 0.435$). Overall, these results suggest that models with integrated video-audio processing gain increased brain alignment from extended temporal context than video-only baselines.

[A2](a): Long windows preferentially benefit higher-order semantic regions, while intermediate windows are optimal for several mid-level temporal ROIs.

We next examine how shorter vs. longer temporal windows differentially affect brain alignment across language, visual, and auditory regions using a voxel-wise window-preference analysis. Specifically, for each voxel, we select the temporal context (clip duration) that results in the highest normalized brain alignment (averaged across subjects) and apply the window-specific color code to the voxel in Fig. 3 (left). We show brain maps for Qwen-2.5-Omni across temporal windows of 3 s, 6 s, 9 s, and 12 s. We observe the following: (i) In language ROIs, posterior temporal lobe (PTL) (and angular gyrus (AG)) show a clear preference for intermediate context (6 s); (ii) Higher-order language ROIs (anterior temporal lobe (ATL), inferior frontal gyrus (IFG), middle frontal gyrus (MFG), orbital IFG (IFGOrb), posterior cingulate cortex (PCC) and dorsomedial prefrontal cortex (dmPFC)) show a strong brain alignment preference for longer context (12 s); (iii) Across ROIs, 9 s rarely emerges as the dominant window. Overall, longer windows are most predictive in PCC/dmPFC, consistent with longer-timescale narrative integration. The low dominance of 9 s in winner-take-all maps does not imply weak performance; rather, 9 s is often competitive but is frequently outperformed by 12 s for many voxels, causing 12 s to dominate the argmax.

Fig. 3 (right) quantifies these effects ROI-wise across language network. We make the following observations (i) Most higher-level language ROIs show a plurality of voxels preferring 12 s, including ATL, IFG, MFG, IFGOrb, PCC, and dmPFC. In contrast, a smaller subset shows a strong intermediate-timescale preference: PTL is best predicted at window 6s, and AG also leans toward 6 s. Notably, 9 s rarely emerges as the plurality winner across ROIs, suggesting that the dominant transitions are from short (3 s) to moderate (6 s) and from moderate (6 s) to long (12 s), rather than a smooth monotonic shift.

Overall, these results support heterogeneous temporal integration across cortex: long windows preferentially benefit higher-order semantic regions, while intermediate windows are optimal for several mid-level temporal ROIs. Together, these results reveal a temporal gradient: shorter windows emphasize local perceptual-linguistic encoding, whereas longer windows capture abstract narrative integration across distributed language and association networks.

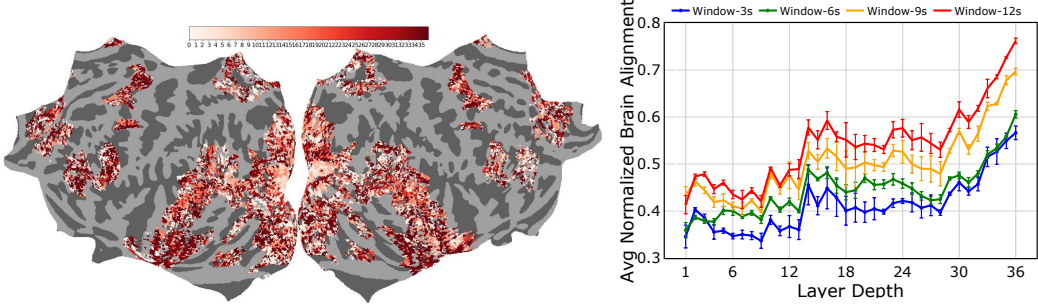


Figure 4: Layer-wise alignment results for Qwen-2.5-Omni: Each voxel is color coded with the MLLM layer number (out of 36) that led to the highest normalized brain alignment. The color bar highlights color codes for each layer. The voxels are projected onto the flattened cortical surface of the ‘fsaverage’ subject. Results for DATE are in Appendix F.

Consistent with the pattern in Fig. 3, the DATE model relative to Qwen-2.5-Omni, we quantitatively observe that the percentage of voxels in the ROIs shows a more even split between intermediate windows (6–9 s) across several ROIs, while 12 s remains the dominant best window across most ROIs (notably PCC/dmPFC) (see Appendix E and Fig. 10). In contrast, the unimodal video baselines show little to no gain in average normalized brain alignment as temporal context increases. Appendix E Fig. 11) shows the brainmap for the unimodal baselines. The voxel-wise maps indicate that longer temporal windows tend to yield higher alignment in higher-order language/association regions, whereas shorter windows are more predictive in early sensory regions.

[A2](b): Layer-wise MLLM representations form a cortical language hierarchy and shift with temporal context.

We investigate how MLLM brain-encoding performance varies across model layers as the temporal context window increases, as shown in Fig. 4 (right). Across all temporal windows, we observe a consistent stratification into three layer groups: early layers (1–12), middle layers (13–28), and late layers (29–36). We find a layer-wise hierarchy: normalized brain alignment generally improves from early to deeper layers across sliding time windows, suggesting progressively more abstract representations in later layers.

Fig. 4 (left) visualizes voxel-wise layer preferences for the 12 s condition, projected onto the fsaverage subject. We observe that (i) early sensory regions (early visual and auditory cortex) align best with lower layers, consistent with shallow representations capturing low-level sensory features; (ii) higher-level visual regions such as lateral occipital complex (LOC) and parahippocampal place area (PPA), and temporal/parietal language ROIs (PTL and AG) tend to align with middle-to-late layers; and (iii) language-related regions such as inferior frontal gyrus (IFG), anterior temporal lobe (ATL), and angular gyrus align most strongly with the deepest layers. Together, these results suggest that MLLMs exhibit a layered representational hierarchy that broadly mirrors cortical processing hierarchies. Layer-wise brain maps for each subject for Qwen-2.5-Omni are shown in Appendix F (Fig. 13). We observe a similar language hierarchy for the DATE model in Appendix F (Fig. 12).

[A3]: Narrative task-specific representations show ROI-specific dissociations in encoding performance.

To investigate which task instructions are more effective in predicting brain activity and whether MLLMs differentiate task-specific representations and provide clear separation in brain regions, we analyze the voxels as follows. For each voxel, we select the task instruction that results in the highest normalized brain alignment and apply the task instruction-specific color code to the voxel Fig. 5 (left). We also report, for each ROI, the fraction of voxels for which each task is optimal (Fig. 5, right).

From Fig. 5 (left), we make the following observations: (i) *Narrative Summary* and *Multiscene Summary* tasks explain a large fraction of voxels across widespread association cortex, consistent with these tasks emphasizing long-range semantic integration over extended narrative context. (ii) *Character Motivation* emerges as the winner in lateral/ventral temporal and occipito-temporal cortex, suggesting that character-centric inference aligns more strongly with regions supporting person-

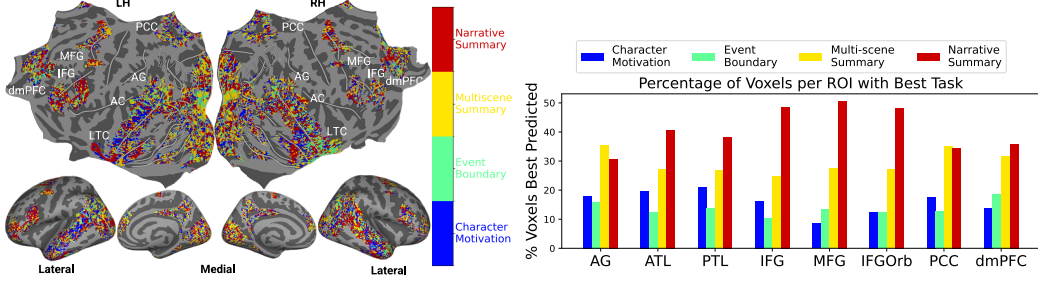


Figure 5: (Left) Each voxel is color-coded with the instruction that led to the highest normalized brain alignment for Qwen-2.5-Omni model. The color bar highlights color codes for each instruction. The voxels are projected onto the flattened cortical surface of the ‘fsaverage’ subject. (Right) Percentage of voxels in each ROI corresponding to each instruction. Results for DATE are in Appendix G.

and situation-level representations grounded in audiovisual content. (iii) *Event Detection* appears comparatively sparse and localized, indicating that boundary/event-focused representations explain fewer voxels overall and may be confined to more specialized subregions. (iv) The strong intermixing of winning tasks within broad territories (rather than a single task dominating everywhere) suggests that task instruction prompts act as functional probes, revealing heterogeneous, task-selective subpopulations of voxels even within the same large-scale networks.

Fig. 5 (right) summarizes task preferences across language ROIs. *Narrative Summary* has highest fractional of voxels in frontal and temporal ROIs such as IFG, MFG, IFGOrb, ATL, PTL) and in dmPFC, indicating that global narrative integration prompts yield representations most predictive of these regions. *Multi-scene Summary* is especially prominent in integrative hubs such as AG and PCC, where it is comparable to *Narrative Summary*. *Character Motivation* contributes a relatively larger share in temporal language ROIs (notably ATL and PTL), whereas *Event Boundary Detection* is rarely the plurality winner, with comparatively higher contributions in dmPFC (and to a lesser extent AG). Overall, integration-focused prompts (Narrative/Multi-scene Summary) dominate higher-order ROIs, while agent-centric prompts (Character Motivation) contribute more in temporal language areas.

We observed similar findings for DATE model, as discussed in Appendix G Fig. 14. Additional interpretability analyses of voxel-wise encoding weights across tasks and context windows are reported in Appendix H (Fig. 15).

[A4]: Maximally activating video clips are stable in visual ROIs but shift with temporal context in higher-order language ROIs.

To select the video clips that elicit the highest response in a given voxel, we used the voxelwise estimated encoding-model weights across temporal windows. For each temporal window w and voxel v , let $\beta_v^{(w)} \in \mathbb{R}^F$ denote the learned weight vector and $x_c^{(w)} \in \mathbb{R}^F$ denote the feature vector for clip c . We scored every clip by the dot product $s_v^{(w)}(c) = \langle \beta_v^{(w)}, x_c^{(w)} \rangle = (\beta_v^{(w)})^\top x_c^{(w)}$, and selected largest scoring $K=10$ clips. These top-ranked clips are those that the encoding model predicts will elicit the strongest responses in voxel v for window w , providing an interpretable characterization of voxel tuning in the model feature space.

Window-conditioned retrieval. We analyze 1000 best-predicted voxels across 4 temporal windows to identify which video clips drive neural responses during long-form movie processing. Fig. 6 shows retrieved clips for representative voxels in visual (LOC, face-selective cortex) and higher-order language regions (AG, PCC) across context windows. We quantify temporal consistency using Jaccard similarity (J) of retrieved videos across window pairs. Visual ROIs show high consistency (LOC: $J=0.50$; Face: $J=0.38$) with category-coherence (object-/shape-dominated for LOC and face/head-dominated for face-selective voxels). But, AG (Win3 → Win12: $\Delta J = 0.094$) and PCC (Win3 → Win12: $\Delta J = -0.153$) exhibit larger shifts in retrieved clips as context length increases, suggesting greater sensitivity to broader semantic and narrative context.

Task-conditioned retrieval. We next examine whether the identity of the narrative-task instruction changes which video clips are predicted to maximally activate voxels within a given ROI. Using the same scoring-and-retrieval procedure as above, we select the top- K clips for ROI-selective voxels



Figure 6: Temporal window conditioned top-K video clips driving voxel responses for Narrative summary task: Results for ROI selective voxels for Subject-1. We identify the top-10 videos from the test stimulus with highest average activation in each temporal window of ROI selective voxels for the AG, PCC, LOC and Face regions. *For visualization, we show only the single highest-ranked video segment in each condition; the images are sampled frames from within that W-second segment.*

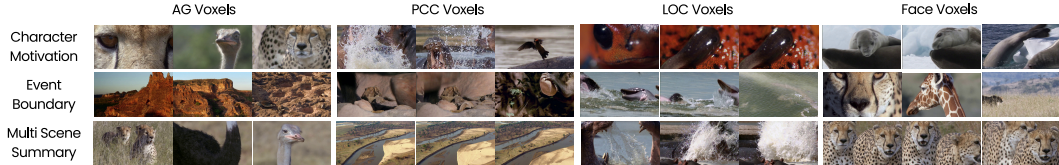


Figure 7: Task conditioned top-K video clips driving voxel responses for longer temporal window (12 s): Results for ROI selective voxels for Subject-1. We identify the top-10 videos from the test stimulus with highest average activation in each temporal window of ROI selective voxels for the AG, PCC, LOC and Face regions. *For visualization, we show only the single highest-ranked video segment in each task; the images are sampled frames from within that segment. Results for narrative summary task are in Fig. 6.*

under each task instruction and visualize the resulting clips for AG, PCC, LOC, and face-selective voxels. Fig. 7 shows retrieved clips under different narrative-task prompts. To quantify task-dependent modulation, we compute Jaccard similarity between retrieved video sets for each ROI under different task instructions. Similar to Window-conditioned retrieval, visual ROIs remain stable across tasks (LOC: $J = 0.42$, Face: $J = 0.38$), whereas AG and PCC vary more across prompts (AG: $J = 0.04$, PCC: $J = 0.13$), indicating that task instructions modulate the semantic/contextual aspects of representations that best align with higher-order regions.

We observe that (i) in category-selective visual ROIs (LOC and face-selective cortex), the retrieved clips remain visually coherent and category-consistent across tasks (e.g., object/texture- and face/animal-head-dominated clips), suggesting that these regions are driven primarily by stable visual content rather than task framing; (ii) in higher-order regions (AG and PCC), the retrieved clips vary more substantially across task instructions, indicating that task prompting modulates the semantic/contextual aspects of the representation that best align with these ROIs. For example, *Character Motivation* tends to retrieve agent-centric clips with salient animals/faces, whereas *Event Boundary* and summarization-style prompts retrieve more context-rich exemplars.

Together with the window-based retrieval (Fig. 6), these results suggest that visual ROIs show stable tuning across both temporal contexts and tasks, whereas higher-order ROIs exhibit stronger task- and context-dependent shifts in the stimuli predicted to drive voxel responses.

6 Discussion and Conclusion

We studied how temporal context and narrative-task prompting influence brain-model alignment during naturalistic movie watching. Using voxel-wise encoding on Movie10 fMRI dataset, we compared two video-audio MLLMs against unimodal baselines and obtained these findings.

First, increasing clip duration (3–12 s) substantially improves brain alignment for video-audio MLLMs but not for unimodal models (Fig. 2). This suggests gains arise from temporal and multimodal integration rather than simply adding frames, highlighting long-form narrative video as a probe of biologically meaningful timescales in MLLMs. **Second**, context-length preferences reveal an ROI-specific temporal gradient: shorter windows (3–6 s) align with perceptual and early language regions (PTL), whereas longer windows align with higher-order integrative regions (PCC/dmPFC/ATL); this

pattern is mirrored in model depth, with deeper layers better predicting higher-level cortex (Figs. 3, 4), indicating a representational hierarchy paralleling cortical processing during movie watching. **Third**, narrative-task instructions produce task-specific, ROI-dependent representations rather than a single generic embedding: different instructions yield distinct voxel/ROI alignment patterns (Fig. 5), and the top-ranked video clips driving voxels differ by ROI and context (Fig. 6, 7). **Fourth**, visual ROIs (LOC, face-selective cortex) show stable clip preferences across windows, while higher-order regions (AG, PCC) exhibit strong context-dependent shifts.

Overall, video–audio MLLMs capture a hierarchy and temporal integration that track cortical processing during narrative processing. Task conditioning provides a useful functional probe of brain-aligned representations. Our results bridge neuroscience studies of long-timescale narrative processing with interpretable evaluations of long ctx. MLLMs.

Impact Statement

This work offers interpretable insights into timescale- and region-specific correspondences between cortical activity and model representations during naturalistic movie watching. For AI community, this work proposes a neuro-grounded evaluation protocol for long-context multimodal models, useful for diagnosing whether architectural changes (temporal modules, fusion) produce representations that behave more like biological integration.

We did not create any new neural recordings data as part of this work. We used the Movie10 dataset which is publicly available without any restrictions. Movie10 dataset can be downloaded from <https://github.com/courtois-neuromod/movie10/tree/33a97c01503315e5e09b3ac07c6ccadb8b887dcf>. Please read their terms of use² for more details. We do not foresee any harmful uses of this technology.

References

Abbott, H. P. *The Cambridge Introduction to Narrative*. Cambridge University Press, 2008.

Aw, K. L. and Toneva, M. Training language models to summarize narratives improves brain alignment. In *The Eleventh International Conference on Learning Representations*, 2023.

Baker, C. M., Burks, J. D., Briggs, R. G., Conner, A. K., Glenn, C. A., Taylor, K. N., Sali, G., McCoy, T. M., Battiste, J. D., O’Donoghue, D. L., et al. A connectomic atlas of the human cerebrum—chapter 7: the lateral parietal lobe. *Operative Neurosurgery*, 15(suppl_1):S295–S349, 2018.

Baldassano, C., Hasson, U., and Norman, K. A. Representation of real-world event schemas during narrative perception. *Journal of Neuroscience*, 38(45):9689–9699, 2018.

Bartlett, F. C. *Remembering: A study in experimental and social psychology*. Cambridge university press, 1995.

Benjamini, Y. and Hochberg, Y. Controlling the false discovery rate: a practical and powerful approach to multiple testing. *Journal of the Royal statistical society: series B (Methodological)*, 57(1):289–300, 1995.

Bertasius, G., Wang, H., and Torresani, L. Is space-time attention all you need for video understanding? In *Proceedings of the International Conference on Machine Learning (ICML)*, July 2021.

Boyle, J. A., Pinsard, B., Boukhddir, A., Belleville, S., Brambatti, S., Chen, J., Cohen-Adad, J., Cyr, A., Fuente, A., Rainville, P., and Bellec, P. The courtois project on neuronal modelling - first data release. In *26th OHBM annual meeting*. Organization for Human Brain Mapping (OHBM), 2020. URL <https://publications.polymtl.ca/50613/>.

Bruner, J. The narrative construction of reality. *Critical inquiry*, 18(1):1–21, 1991.

²<https://docs.cneuromod.ca/en/latest/ACCESS.html>

Caucheteux, C. and King, J.-R. Brains and algorithms partially converge in natural language processing. *Communications Biology*, 5(1):134, 2022.

Conover, W. J. *Practical nonparametric statistics*, volume 350. John Wiley & Sons, 1999.

Deniz, F., Nunez-Elizalde, A. O., Huth, A. G., and Gallant, J. L. The representation of semantic information across human cerebral cortex during listening versus reading is invariant to stimulus modality. *Journal of Neuroscience*, 2019.

Desai, R. H., Tadimeti, U., and Riccardi, N. Proper and common names in the semantic system. *Brain Structure and Function*, 228(1):239–254, 2023.

Dong, D. T. and Toneva, M. Interpreting multimodal video transformers using brain recordings. In *ICLR 2023 Workshop on Multimodal Representation Learning: Perks and Pitfalls*, 2023a.

Dong, D. T. and Toneva, M. Vision-language integration in multimodal video transformers (partially) aligns with the brain. *arXiv preprint arXiv:2311.07766*, 2023b.

Genovese, C. R. A bayesian time-course model for functional magnetic resonance imaging data. *Journal of the American Statistical Association*, 95(451):691–703, 2000.

Glasser, M. F., Coalson, T. S., Robinson, E. C., Hacker, C. D., Harwell, J., Yacoub, E., Ugurbil, K., Andersson, J., Beckmann, C. F., Jenkinson, M., et al. A multi-modal parcellation of human cerebral cortex. *Nature*, 536(7615):171–178, 2016.

Goldstein, A., Zada, Z., Buchnik, E., Schain, M., Price, A., Aubrey, B., Nastase, S. A., Feder, A., Emanuel, D., Cohen, A., et al. Shared computational principles for language processing in humans and deep language models. *Nature Neuroscience*, 25(3):369–380, 2022.

Goldstein, A., Wang, H., Niekerken, L., Schain, M., Zada, Z., Aubrey, B., Sheffer, T., Nastase, S. A., Gazula, H., Singh, A., et al. A unified acoustic-to-speech-to-language embedding space captures the neural basis of natural language processing in everyday conversations. *Nature Human Behaviour*, pp. 1–15, 2025.

Gupta, P., Jiao, C., Yeh, Y.-T., Mehri, S., Eskenazi, M., and Bigham, J. P. Instructdial: Improving zero and few-shot generalization in dialogue through instruction tuning. *arXiv preprint arXiv:2205.12673*, 2022.

Honey, C. J., Thesen, T., Donner, T. H., Silbert, L., Carlson, C., Devinsky, O., Doyle, W., Rubin, N., Heeger, D. J., and Hasson, U. Slow cortical dynamics and the accumulation of information over long timescales. *Neuron*, 76:423–434, 2012.

Huth, A. G., De Heer, W. A., Griffiths, T. L., Theunissen, F. E., and Gallant, J. L. Natural speech reveals the semantic maps that tile human cerebral cortex. *Nature*, 532(7600):453–458, 2016.

Huth, A. G., Nishimoto, S., Vu, A. T., and Dupre La Tour, T. Gallant lab natural short clips 3t fmri data. *G-Node doi*, 10, 2022.

Jain, S. and Huth, A. G. Incorporating context into language encoding models for fmri. In *NIPS*, pp. 6629–6638, 2018.

Khosla, M., Ngo, G. H., Jamison, K., Kuceyeski, A., and Sabuncu, M. R. Cortical response to naturalistic stimuli is largely predictable with deep neural networks. *Science Advances*, 7(22):eabe7547, 2021.

Lahner, B., Dwivedi, K., Iamshchinina, P., Graumann, M., Lascelles, A., Roig, G., Gifford, A. T., Pan, B., Jin, S., Ratan Murty, N. A., et al. Modeling short visual events through the bold moments video fmri dataset and metadata. *Nature Communications*, 15(1):6241, 2024.

Lerner, Y., Honey, C. J., Silbert, L. J., and Hasson, U. Topographic mapping of a hierarchy of temporal receptive windows using a narrated story. *Journal of Neuroscience*, 31(8):2906–2915, 2011.

Milton, C. K., Dhanaraj, V., Young, I. M., Taylor, H. M., Nicholas, P. J., Briggs, R. G., Bai, M. Y., Fonseka, R. D., Hormovas, J., Lin, Y.-H., et al. Parcellation-based anatomic model of the semantic network. *Brain and Behavior*, 11(4):e02065, 2021.

Nakagi, Y., Matsuyama, T., Koide-Majima, N., Yamaguchi, H., Kubo, R., Nishimoto, S., and Takagi, Y. The brain tells a story: Unveiling distinct representations of semantic content in speech, objects, and stories in the human brain with large language models. *bioRxiv*, pp. 2024–02, 2024.

Oota, S. R., Çelik, E., Deniz, F., and Toneva, M. Speech language models lack important brain-relevant semantics. In *Proceedings of the 62nd Annual Meeting of the Association for Computational Linguistics (Volume 1: Long Papers)*, pp. 8503–8528. Association for Computational Linguistics, 2024. URL <https://aclanthology.org/2024.acl-long.462>.

Oota, S. R., Chen, Z., Gupta, M., Surampudi, B. R., Jobard, G., Alexandre, F., and Hinaut, X. Deep neural networks and brain alignment: Brain encoding and decoding (survey). *Transactions on Machine Learning Research*, 2025a. ISSN 2835-8856. URL <https://openreview.net/forum?id=YxKJihRcb>. Survey Certification.

Oota, S. R., Jindal, A. R., Mondal, I., Pahwa, K., GNVV, S. S. S. N., Shrivastava, M., Singh, M. K., Surampudi, B. R., and Gupta, M. Correlating instruction-tuning (in multimodal models) with vision-language processing (in the brain). In *The Thirteenth International Conference on Learning Representations*, 2025b.

Oota, S. R., Pahwa, K., Jindal, P., Namburi, S. S. S., Singh, M., Chakraborty, T., Raju, B. S., and Gupta, M. Instruction-tuned video-audio models elucidate functional specialization in the brain. *arXiv preprint arXiv:2506.08277*, 2025c.

Oota, S. R., Pahwa, K., mounika marreddy, Singh, M. K., Gupta, M., and Surampudi, B. R. Multi-modal brain encoding models for multi-modal stimuli. In *The Thirteenth International Conference on Learning Representations*, 2025d.

Popham, S. F., Huth, A. G., Bilenko, N. Y., Deniz, F., Gao, J. S., Nunez-Elizalde, A. O., and Gallant, J. L. Visual and linguistic semantic representations are aligned at the border of human visual cortex. *Nature Neuroscience*, 24(11):1628–1636, 2021.

Rabinowitz, N., Perbet, F., Song, F., Zhang, C., Eslami, S. M. A., and Botvinick, M. Machine theory of mind. In Dy, J. and Krause, A. (eds.), *Proceedings of the 35th International Conference on Machine Learning*, volume 80 of *Proceedings of Machine Learning Research*, pp. 4218–4227. PMLR, 10–15 Jul 2018. URL <https://proceedings.mlr.press/v80/rabinowitz18a.html>.

Reddy, A. J. and Wehbe, L. Can fmri reveal the representation of syntactic structure in the brain? *Advances in Neural Information Processing Systems*, 34:9843–9856, 2021.

Sartetaki, C., Roig, G., Snoek, C. G., and Groen, I. I. One hundred neural networks and brains watching videos: Lessons from alignment. In *The Thirteenth International Conference on Learning Representations*, 2025. URL <https://openreview.net/pdf?id=LM4PYXBId5>.

Schrimpf, M., Blank, I. A., Tuckute, G., Kauf, C., Hosseini, E. A., Kanwisher, N., Tenenbaum, J. B., and Fedorenko, E. The neural architecture of language: Integrative modeling converges on predictive processing. *Proceedings of the National Academy of Sciences*, 2021.

Schwartz, O. et al. Neuroai and the study of representation: bridging cognitive neuroscience and machine learning, 2022. Review/position paper.

Simony, E., Honey, C. J., Chen, J., Lositsky, O., Yeshurun, Y., Wiesel, A., and Hasson, U. Dynamic reconfiguration of the default mode network during narrative comprehension. *Nature communications*, 7(1):12141, 2016.

Subramaniam, V., Wang, C., Barbu, A., Kreiman, G., and Katz, B. Revealing vision-language integration in the brain with multimodal networks. In *International Conference on Machine Learning*. International Conference on Machine Learning (ICML), 2024.

Tang, J., Du, M., Vo, V., Lal, V., and Huth, A. Brain encoding models based on multimodal transformers can transfer across language and vision. *Advances in Neural Information Processing Systems*, 36, 2024.

Toneva, M. and Wehbe, L. Interpreting and improving natural-language processing (in machines) with natural language-processing (in the brain). *Advances in Neural Information Processing Systems*, 32, 2019.

Tong, Z., Song, Y., Wang, J., and Wang, L. Videomae: Masked autoencoders are data-efficient learners for self-supervised video pre-training. *Advances in Neural Information Processing Systems*, 35:10078–10093, 2022.

Vaidya, A., Jain, S., and Huth, A. Self-supervised models of audio effectively explain human cortical responses to speech. In *International Conference on Machine Learning*, pp. 21927–21944. PMLR, 2022.

Wehbe, L., Murphy, B., Talukdar, P., Fyshe, A., Ramdas, A., and Mitchell, T. Simultaneously uncovering the patterns of brain regions involved in different story reading subprocesses. *PLoS one*, 11, 2014.

Xu, J., Guo, Z., He, J., Hu, H., He, T., Bai, S., Chen, K., Wang, J., Fan, Y., Dang, K., et al. Qwen2.5-omni technical report. *arXiv preprint arXiv:2503.20215*, 2025.

Yuan, C., Yang, Y., Yang, Y., and Cheng, Z. Date: Dynamic absolute time enhancement for long video understanding. *arXiv preprint arXiv:2509.09263*, 2025.

Zacks, J. M. and Swallow, K. M. Event segmentation. *Current Directions in Psychological Science*, 16(2):80–84, 2007. doi: 10.1111/j.1467-8721.2007.00480.x. URL <https://doi.org/10.1111/j.1467-8721.2007.00480.x>. PMID: 22468032.

Zellers, R., Lu, X., Hessel, J., Yu, Y., Park, J. S., Cao, J., Farhadi, A., and Choi, Y. Merlot: Multimodal neural script knowledge models. *Advances in neural information processing systems*, 34:23634–23651, 2021.

Overview of Appendix Sections

Appendix A	Dataset and Detailed sub-ROIs of language, visual and auditory regions
Appendix B	Cross-subject prediction accuracy
Appendix C	Description of Narrative video understanding tasks
Appendix D	Implementation details for reproducibility.
Appendix E	Window-wise Voxel Alignment for DATE and TimeSformer
Appendix F	Layer-wise Analysis for DATE
Appendix G	Task-wise Voxel Alignment for DATE
Appendix H	Interpretability Analysis for DATE and TimeSformer
Appendix I	Statistical Significance

A Dataset and Detailed sub-ROIs of language, visual and auditory regions

Brain imaging dataset. We experiment with Movie10 (Boyle et al., 2020), a multimodal naturalistic fMRI dataset, obtained from the Courtois NeuroMod databank. This dataset was collected while four human subjects (s_1, s_2, s_3, s_5 ; data for s_4 and s_6 is not public) passively watched four different movies: *The Bourne supremacy* (~ 100 mins), *The wolf of wall street* (~ 170 mins), *Hidden figures* (~ 120 mins) and *Life* (~ 50 mins). Among these, *Hidden figures* and *Life* are repeated twice, with the repeats used for testing and the remaining movies for training. In this work, we use *Life* movies for testing where we average the two repetitions to reduce noise in brain data. This dataset is one of the largest publicly available multimodal fMRI datasets in terms of the number of samples per participant. It includes 4024 TRs (Time Repetitions) of *The Bourne supremacy* and 6993 TRs of *The wolf of wall street* for training and 2013 TRs of *Life* as test data. We build encoding models where the train and test sets are totally disjoint. The fMRI data is collected every 1.49 seconds ($= 1$ TR).

The dataset is already preprocessed and projected onto the surface space (“fsaverage6”). We use the multimodal parcellation of the human cerebral cortex based on the Glasser Atlas (which consists of 180 regions of interest in each hemisphere) to report the ROI (region of interest) analysis for the brain maps (Glasser et al., 2016). This includes four visual processing regions (early visual cortex (EVC), object-related areas (LOC), face-related areas (OFA) and scene-related areas (PPA)), one early auditory area (AC), and eight language-relevant regions, encompassing broader language regions: angular gyrus (AG), anterior temporal lobe (ATL), posterior temporal lobe (PTL), inferior frontal gyrus (IFG), inferior frontal gyrus orbital (IFGOrb), middle frontal gyrus (MFG), posterior cingulate cortex (PCC) and dorsal medium prefrontal cortex (dmPFC), based on the Fedorenko lab’s language parcels (Milton et al., 2021; Desai et al., 2023).

The data covers seven brain regions of interest (ROIs) in the human brain with the following subdivisions: (i) early visual (EV: V1, V2, V3, V3B, and V4); (ii) object-related areas (LO1 and LO2); (iii) face-related areas (OFA), (iv) scene-related areas (PPA), (v) middle temporal (MT: MT, MST, LO3, FST and V3CD), (vi) late language regions, encompassing broader language regions: angular gyrus (AG: PFm, PGs, PGi, TPOJ2, TPOJ3), lateral temporal cortex (LTC: STSda, STSva, STGa, TE1a, TE2a, TGv, TGd, A5, STSdp, STSvp, PSL, STV, TPOJ1), inferior frontal gyrus (IFG: 44, 45, IFJa, IFSp) and middle frontal gyrus (MFG: 55b) (Baker et al., 2018; Milton et al., 2021; Desai et al., 2023).

B Cross-subject prediction accuracy

We follow the method introduced by Schrimpf et al. (2021) to estimate how well brain activity in one individual can be predicted from others, using the Movie10 fMRI dataset. Starting with data from n participants (e.g., $n = 4$), for each subject $s \in (s_1, s_2, s_3, s_5)$ is chosen as the prediction target and the other three are used to predict this target, we use a voxel-wise encoding model (see Sec. 5.1) to predict one participant’s response from others. For every combination, one participant was randomly chosen as the target, and the model was trained to predict their brain responses using data from the remaining $n - 1$ participants. This gave us an average prediction score (correlation) for each voxel at each participant. To extrapolate to infinitely many humans and thus to obtain the highest possible (most conservative) estimate, as suggested by Schrimpf et al. (2021), we fit the equation $v = v_0 \times \left(1 - e^{-\frac{x}{\tau_0}}\right)$ where x is each subsample’s number of participants, v is each subsample’s correlation score and v_0 and τ_0 are the fitted parameters. This fitting was performed for each sensor

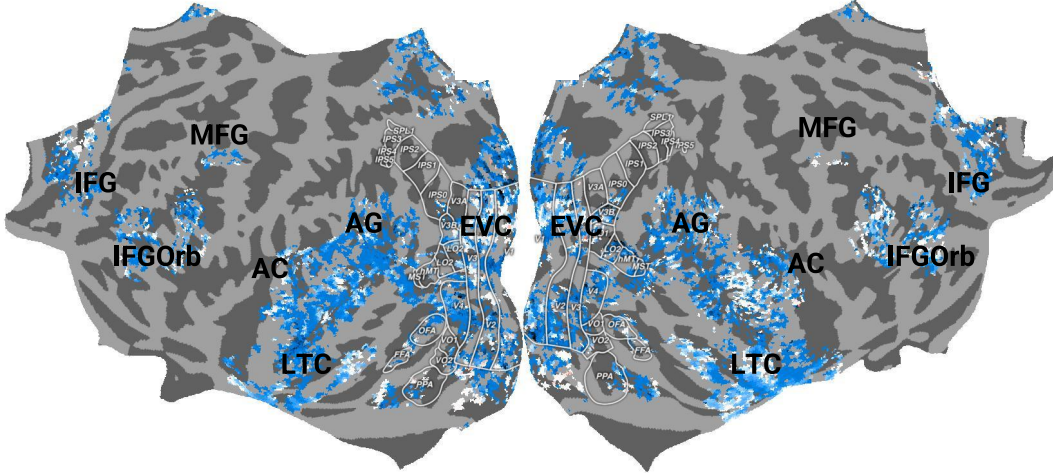


Figure 8: Flattened cortical surfaces for language-, visual- and auditory-selective regions displayed on the ‘fsaverage’ surface, used as the mask for all participants.

independently with 100 bootstraps each to estimate the variance where each bootstrap draws x and v with replacement. The final ceiling value was the median of the per-voxel ceilings v_0 .

Fig. 9 shows the estimated cross-subject prediction accuracy for all four participants for the naturalistic movie watching. Pearson correlation scores for each voxel in each subject are projected onto the subject’s flattened cortical surface. The plots show that across all subjects higher activity is observed in the language and visual regions with a max correlation up to 0.4 implying that data has low noise and low cross-subject variability.

C Description of Narrative video understanding tasks

Each task addresses a unique aspect of narrative meaning. Character Motivation captures implicit beliefs and goals of agents Rabinowitz et al. (2018). Event Boundary Detection identifies fine-grained change points critical for temporal segmentation Zacks & Swallow (2007). Multi-Scene Summary integrates local events across broader spans. Narrative Summary consolidates long-range relational structure and thematic coherence Bartlett (1995). Removing any one task leaves certain forms of information unrecoverable from the others (e.g., agent beliefs, change points, relational links, or fine event details), establishing necessity. Conversely, under the decomposition and representability assumptions, the four tasks together span the relevant semantic space, up to a simple readout, establishing sufficiency.

D Implementation details for reproducibility

All feature extraction experiments were conducted on a machine equipped with an NVIDIA A100 GPU with 80 GB of GPU RAM, partitioned into two devices of 40 GB each. The voxelwise encoding models were trained on NVIDIA GeForce RTX 3050 GPU with 4GB of GPU RAM. We used banded ridge-regression with the following parameters: MSE loss function; L2-decay (λ) varied from 10^{-1} to 10^3 ; the best λ was chosen by tuning on validation data that comprised a randomly chosen 10% subset from the train set used only for hyper-parameter tuning.

E Window-wise Voxel Alignment for DATE and TimeSformer

To test whether the temporal-context effects generalize beyond Qwen-2.5-Omni, we repeat the same window-wise voxel analysis using the DATE model. As in the main analysis, for each voxel we select the temporal window length (3 s, 6 s, 9 s, or 12 s) that yields the highest normalized brain alignment, and visualize the resulting best-window map on the fsaverage surface along with the ROI-wise distribution of best windows (Appendix Fig. 10).

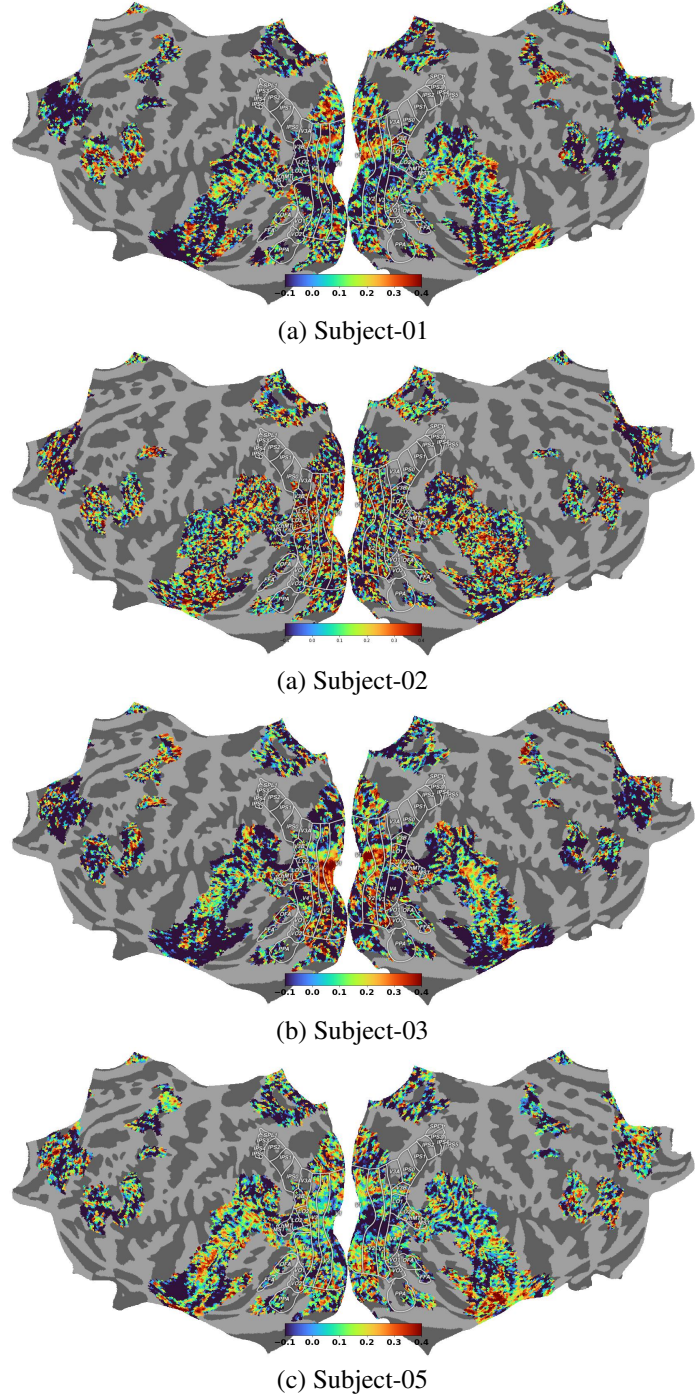


Figure 9: Estimated cross-subject prediction accuracy for all four participants for the naturalistic movie watching. Pearson correlation scores for each voxel in each subject are projected onto the subject’s flattened cortical surface.

Qualitatively, as shown in Fig. 10 (top), DATE exhibits a similar temporal gradient to Qwen-2.5-Omni: shorter-to-intermediate windows (3–6 s) account for a larger share of best-predicted voxels in more perceptual and “local” regions, while longer windows (12 s) dominate in higher-order semantic/integrative regions. In particular, regions such as PCC and dmPFC show a preference for the longest window, consistent with longer-timescale narrative integration. Likewise, several language-selective ROIs (e.g., ATL, IFG, MFG, and IFGOrb) show a clear shift toward longer context windows, whereas PTL retain a comparatively stronger contribution from shorter windows, while AG shows

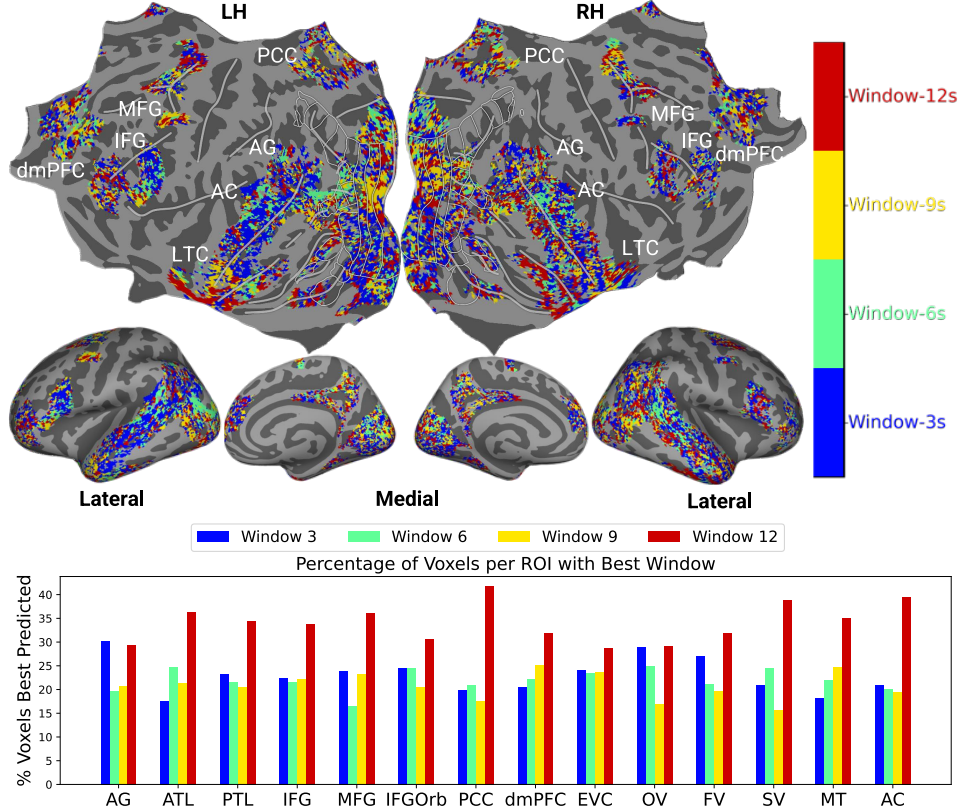


Figure 10: DATE model results: Each voxel is color-coded with the video duration (window length) that led to the highest normalized brain alignment with the DATE model. The color bar highlights color codes for each window length. (Top) The voxels are projected onto the flattened cortical surface of the ‘fsaverage’ subject. (Bottom): Percentage of voxels in each ROI corresponding to each window length.

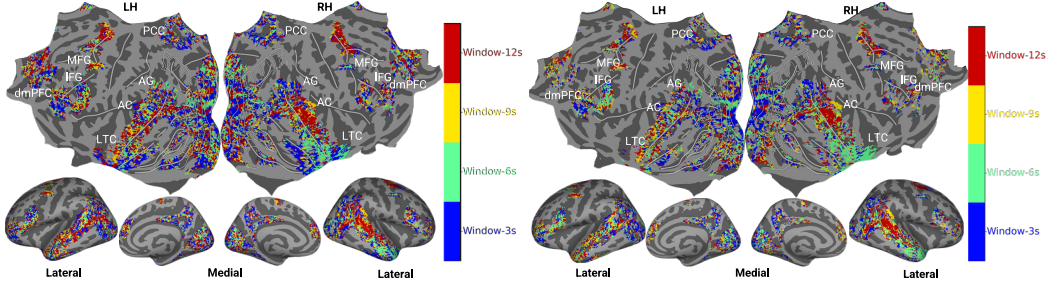


Figure 11: Unimodal video baselines (TimesFormer: Left, and VideoMAE: Right): Each voxel is color-coded with the video duration (window length) that led to the highest normalized brain alignment with the Unimodal video baselines. The color bar highlights color codes for each window length. (Left) The voxels are projected onto the flattened cortical surface of the ‘fsaverage’ subject.

both shorter and longer windows dominance, suggesting that parts of the temporal language system are optimally predicted at shorter timescales. Visual and auditory ROIs show weaker monotonic shifts overall, with early visual cortex appearing comparatively mixed across windows. The ROI-wise histogram (Fig. 10, bottom) further supports these observations, showing that 12 s is the most frequent best window across many higher-order ROIs, while 3–6 s windows contribute more substantially in PTL/AG and several sensory-selective regions. Together, these results indicate that DATE captures heterogeneous temporal integration across cortex in a manner consistent with the main findings, reinforcing that long-context gains in brain alignment reflect model representations that better support long-timescale narrative processing rather than simply increased visual input length.

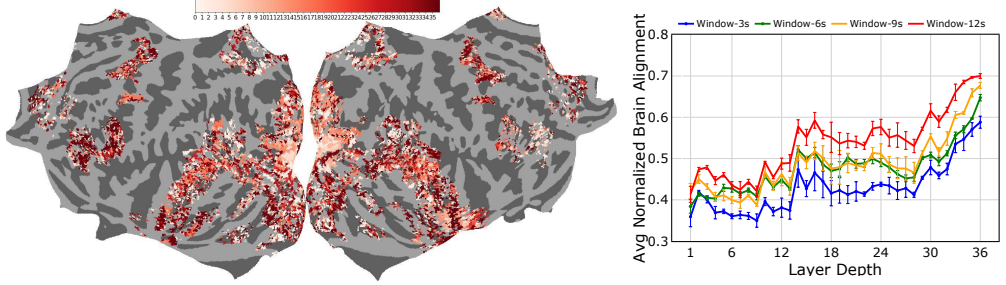


Figure 12: Layer-wise alignment results for DATE: Each voxel is color coded with the MLLM layer number (out of 36) that led to the highest normalized brain alignment. The color bar highlights color codes for each layer. The voxels are projected onto the flattened cortical surface of the ‘fsaverage’ subject.

F Layer-wise Analysis for DATE

We investigate how MLLM brain-encoding performance varies across model layers as the temporal context window increases, as shown in Fig. 12 (right). Across all temporal windows, we observe a consistent stratification into three layer groups: early layers (1–12), middle layers (13–28), and late layers (29–36). Overall, normalized brain alignment increases with longer sliding-window context, indicating that MLLMs benefit from long-range temporal information compared to shorter windows (e.g., 3 s and 6 s). We also find a layer-wise hierarchy: alignment generally improves from early to deeper layers across windows, suggesting progressively more abstract representations in later layers.

Fig. 12 (left) visualizes voxel-wise layer preferences for the 12 s condition, projected onto the *fsaverage* subject. We observe that (i) early sensory regions (early visual and auditory cortex) align best with lower layers, consistent with shallow representations capturing low-level sensory features; (ii) higher-level visual regions such as lateral occipital complex (LOC) and parahippocampal place area (PPA), and temporal/parietal language ROIs (PTL and AG) tend to align with middle-to-late layers; and (iii) language-related regions such as inferior frontal gyrus (IFG), anterior temporal lobe (ATL), and angular gyrus align most strongly with the deepest layers. Together, these results suggest that MLLMs exhibit a layered representational hierarchy that broadly mirrors cortical processing hierarchies.

G Task-wise Voxel Alignment for DATE

To test whether the task-specific dissociations generalize beyond Qwen-2.5-Omni, we repeat the voxel-wise winner-task analysis using the DATE model. For each voxel, we select the narrative-task instruction that yields the highest normalized brain alignment and visualize the resulting winner-task maps on the *fsaverage* surface (Fig. 14) (top). We additionally quantify, for each ROI, the percentage of voxels for which each task is optimal (Fig. 14 (bottom)).

Fig. 14 (top) shows that DATE exhibits a qualitatively similar task-based organization: (i) Both *Narrative Summary* and *Multi-scene Summary* explain a large fraction of voxels across widespread association cortex, consistent with these prompts emphasizing long-range semantic integration; (ii) *Character Motivation* more frequently emerges in lateral temporal and occipito-temporal regions, suggesting stronger alignment with regions supporting person- and situation-level inference grounded in audiovisual content; and (iii) *Event Boundary* is comparatively sparse overall, but appears more prominently in select higher-order territories, indicating more specialized and localized boundary-related tuning rather than broad dominance.

The ROI-wise histogram (Fig. 14 (bottom)) further supports these observations. *Multi-scene Summary* is the plurality winner across many ROIs (including several language/association ROIs such as AG/ATL/MFG/IFGOrb, and multiple visual ROIs), indicating that multi-scene integration prompts capture representations that are broadly predictive across networks. In contrast, *Narrative Summary* shows comparatively stronger contributions in some integrative ROIs (e.g., PPA and several frontal/temporal language ROIs), suggesting that global narrative compression preferentially matches higher-order semantic integration demands. *Character Motivation* accounts for the largest share of best-predicted voxels in more “local” regions such as LOC (and a substantial fraction in PTL),

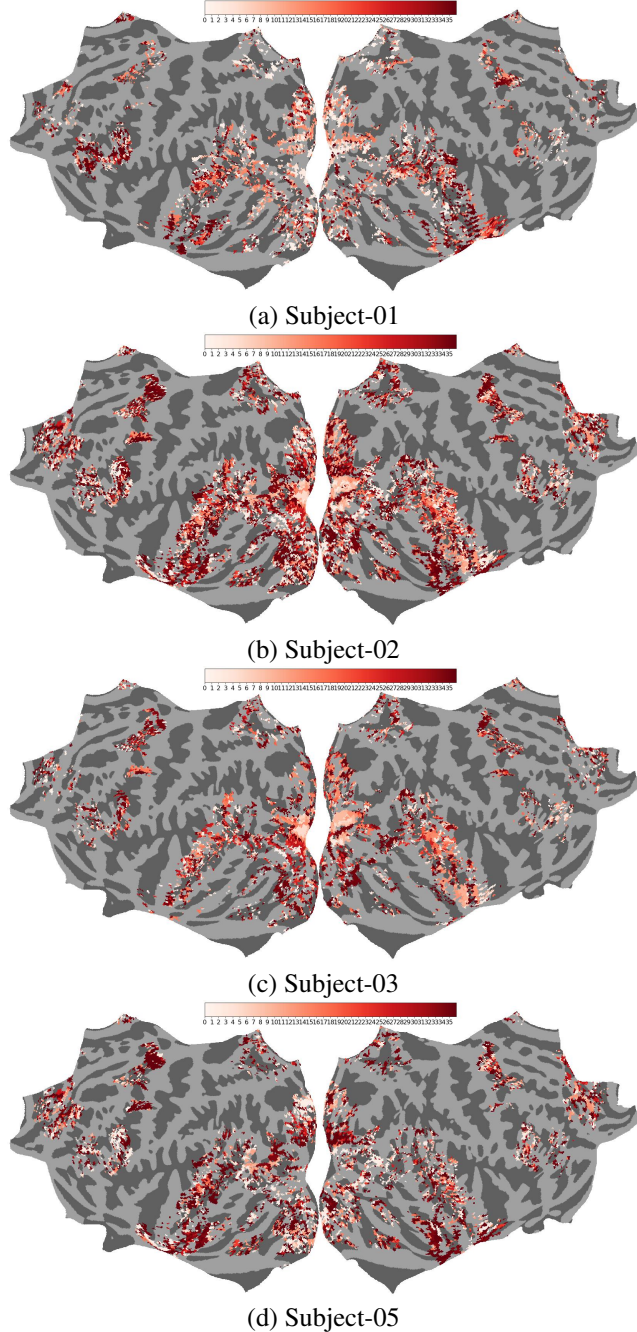


Figure 13: Qwen2.5-Omni: Each voxel is color coded with the video MLLM layer number (out of 36) that led to the highest normalized brain alignment. The color bar highlights color codes for each layer. The voxels are projected onto the flattened cortical surface of each subject on ‘fsaverage’ surface.

consistent with character/agent-centric prompts aligning with regions sensitive to entity-level cues. Finally, *Event Boundary* contributes relatively more in dmPFC and PCC than in most other ROIs, consistent with boundary-related structure being distributed but not the dominant explanatory factor in most regions.

Overall, DATE reproduces the main qualitative conclusion that narrative-task prompting acts as a functional probe: different prompts yield distinct, ROI-specific patterns of brain alignment rather than a single task dominating everywhere.

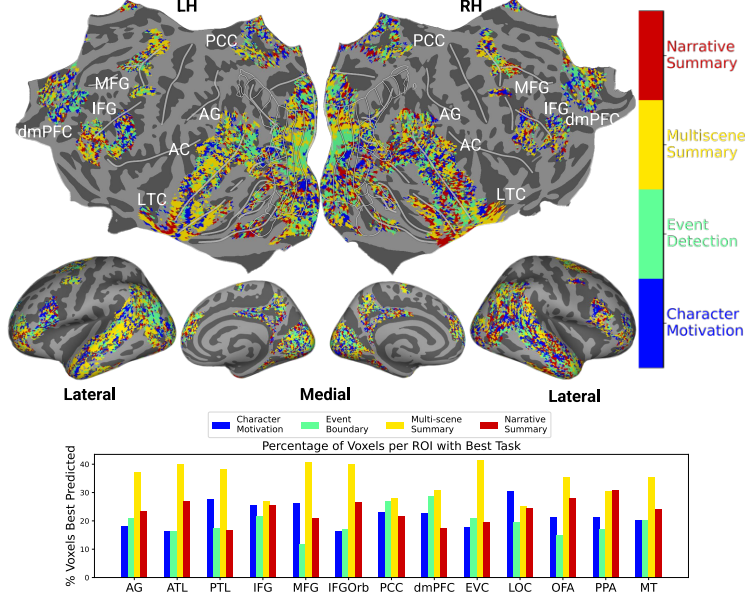


Figure 14: DATE model results: Each voxel is color-coded with the video duration (window length) that led to the highest normalized brain alignment with the DATE model. The color bar highlights color codes for each window length. (Top) The voxels are projected onto the flattened cortical surface of the ‘fsaverage’ subject. (Bottom): Percentage of voxels in each ROI corresponding to each window length.

H Interpretability Analysis for Qwen2.5-Omni and DATE

Fig. 15 shows a 16×16 similarity matrix comparing the voxel-wise encoding weight patterns across 4 tasks \times 4 temporal window lengths within language and visual voxels. We make the following observations: (i) Task identity drives the largest differences in voxel-wise tuning (cross-task similarity is low). (ii) Increasing temporal context tends to make weight patterns more consistent within a task, especially for multi-scene integration and narrative, while event boundary remains relatively weakly consistent across windows. (iii) Even within a task, correlations are not high, implying that context length meaningfully reshapes the learned voxel-feature mapping rather than merely scaling it.

I Statistical Significance

To determine if normalized predictivity scores are significantly higher than chance, we run a permutation test using blocks of 10 contiguous fMRI TRs (considering the slowness of hemodynamic response) rather than individual TRs. By permuting predictions 5000 times, we create an empirical distribution for chance performance, from which we estimate p-value of the actual performance. The choice of these specific permutation test configurations is based on established methodologies in previous research (Deniz et al., 2019; Reddy & Wehbe, 2021; Oota et al., 2024). To estimate the statistical significance of performance differences, such as between the model’s predictions and chance or residual predictions and chance, we utilized the Wilcoxon signed-rank test (Conover, 1999), applying it to the mean normalized predictivity for the participants. Finally, the Benjamini-Hochberg False Discovery Rate (FDR) correction for multiple comparisons (Benjamini & Hochberg, 1995) is used for all the tests (appropriate because fMRI data is considered to have positive dependence (Genovese, 2000)).

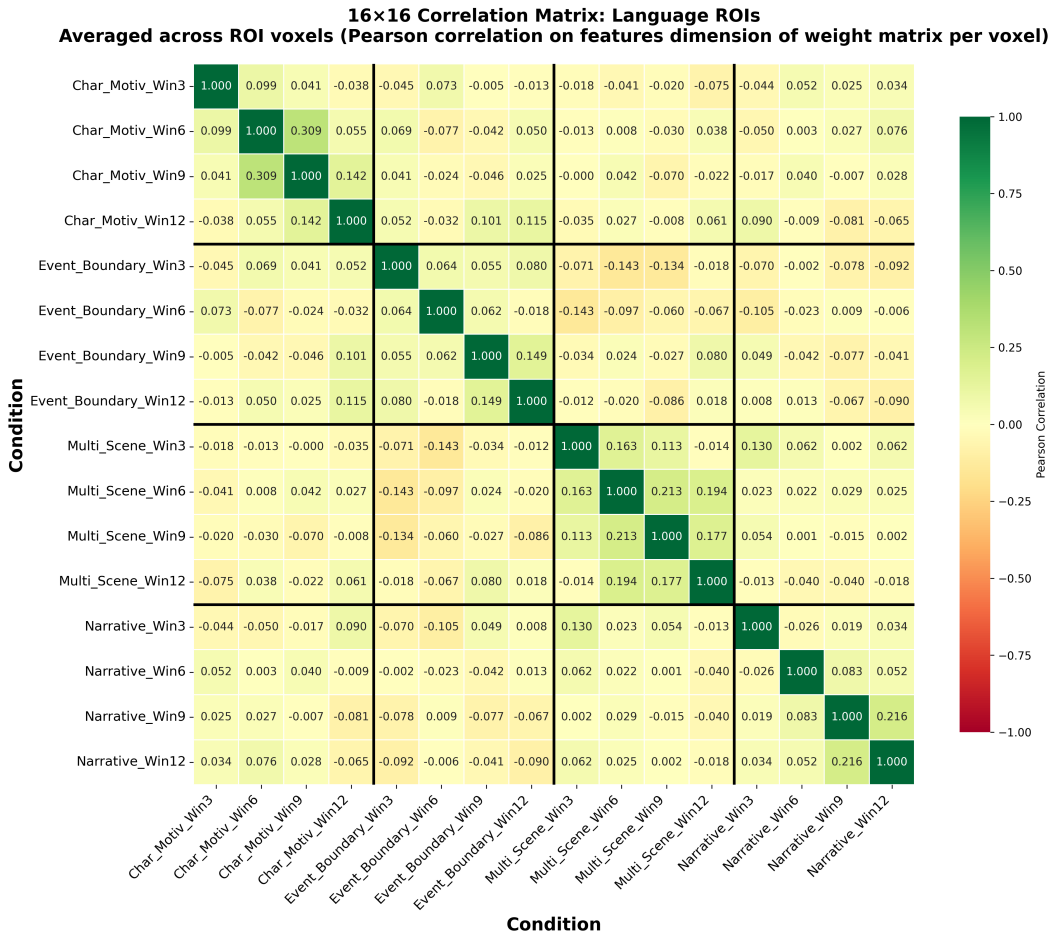


Figure 15: A 16×16 similarity matrix comparing the voxel-wise encoding weight patterns across 4 tasks × 4 temporal windows within language and visual voxels.